Effect of surface roughness and chemistry on the adhesion and durability of a steel-epoxy adhesive interface

van Dam, Joost; Abrahami, ST; Yilmaz, A; Gonzalez-Garcia, Y; Terryn, H; Mol, Arjan

Contents lists available at ScienceDirect

International Journal of Adhesion and Adhesives

Effect of surface roughness and chemistry on the adhesion and durability of a steel-epoxy adhesive interface

J.P.B. van Dam [a], S.T. Abrahami [b], A. Yilmaz [a], Y. Gonzalez-Garcia [a], H. Terryn [a,b], J.M.C. Mol [a,*]

[a] Delft University of Technology, Department of Materials Science and Engineering, Mekelweg 2, 2628, CD Delft, the Netherlands
[b] Department of Materials and Chemistry, Research Group Electrochemical and Surface Engineering (SURF), Vrije Universiteit Brussel, Pleinlaan 2, B-1050, Brussels, Belgium

ARTICLE INFO

ABSTRACT

This work focuses on the effect of surface roughness and surface chemistry on the initial adhesion strength and corrosive de-adhesion properties of adhesive bonds. The adherend used in this study is a S690 low-alloy steel whereas the adhesive is a 2-component epoxy-amine adhesive (Araldite 2015). The steel surface is subjected to different surface pre-treatment methods such as mechanical abrasion, grit blasting, zirconium conversion treatment and silane treatment. The effect of these different pre-treatments on the surface morphology, roughness and chemistry is addressed. Single-lap joint tests were performed at ambient conditions to assess the initial bond strength of the joint. Static wedge tests were performed in saltwater immersions to study the environmental ageing of the adhesive joints. Unloaded delamination of adhesive films from the steel surface was studied by means of scanning Kelvin probe (SKP) at high relative humidity. This unique combination of different techniques allows thorough evaluations of the bond performance under different environmental and loading conditions. Experimental results indicate that surface roughening plays an important role in the initial adhesion in the single-lap joint test but a minor role in the durability of the bonded steel surfaces. The improved initial adhesion is mainly attributed to the increased interfacial bond area at higher surface roughness. The presence of complex texture or morphology shows a more profound effect than the average roughness on both the initial adhesion and the durability of the interfacial adhesion. The results from the static wedge test show the large contribution of mechanical interlocking, caused by texturing of the surface, on the durability of the interfacial adhesion. In the absence of complex texture, surfaces with altered chemistry by zirconium- or silane treatment exhibit a significant increase of the initial bonding strength due to enhanced physicochemical interactions across the interface. Assessment of the interfacial delamination kinetics by SKP show that despite the absence of any surface topography, chemically altered surfaces prove to have higher resistance to delamination.

1. Introduction

The combined use of composite materials and high strength steel in highly loaded structures in the maritime and offshore industry provides many advantages, such as significantly increased strength-to-weight ratio and improved corrosion resistance. Adhesive bonding is already widely applied as a joining method for dissimilar materials in the automotive, aircraft and microelectronic industries, replacing conventional joining techniques such as welding, bolting and riveting [1,2]. Yet, under marine conditions environmental attack of the interface by saline water causes significant degradation of the steel adhesive interface and thereby of the mechanical strength of the joint. This serious

limitation in the durability is the major reason for the limited use of adhesives in these industries so far. In order to obtain higher and satisfactory levels of bond strength and resistance to environmental attack, some form of surface pre-treatment is necessary. The main purpose of surface pre-treatments is to remove all contaminants and weak layers from the surface, acquire a large surface area and assure all bonding mechanisms responsible for adhesion are triggered (mechanical, physical and chemical).

Many studies have therefore been dedicated to the development of suitable surface pre-treatments. A combination of surface analysis and destructive mechanical testing, with varying geometries, is commonly used to measure the effect of surface pre-treatments on both the initial-

and the residual adhesion strength after environmental ageing [3,4]. Via such approach, Critchlow et al. found that a range of conversion coatings provided highly modified oxides, in terms of both stable chemistry and complex texture [5]. The highly improved adhesion was assigned to a combination of possible "interphase" formation, micro-rough texture and the chemical stability of the oxide. The empirical test approach utilized by Critchlow et al. provides important information on the mechanical performance of adhesive joints for a particular bonded system and possible causes. However, it does not provide fundamental information about the contribution or effect of individual surface properties on interfacial adhesion. The texturing or roughening of the surfaces prior to bonding, e.g. by chemical treatment or mechanical abrasion, enhances the strength of the adhesive joint, yet the relationship between roughness and adhesion is not fully understood. The relation can either be attributed to the large effective surface area or it can provide some degree of mechanical interlocking. Therefore, several studies have focused on describing the roughness by means of different parameters and linking them to mechanical strength.

The effect of different steel surface roughnesses on the adhesive bond strength by profilometry and tensile testing was studied by Ghumatkar et al. [6]. Different roughnesses were created using mechanical abrasion and an optimum in average roughness was found at 1.97 μm. The improved adhesion was assigned to possible mechanical interlocking. Zielecki et al. studied the effect of both surface roughness and topography on the mechanical strength of steel-to-steel adhesive joints [7]. In their conclusions they state that the shear strength of the joints is proportional to the effective interfacial surface area, thereby rejecting the concept of additional mechanical interlocking. Besides mechanical testing to study the initial and residual adhesion, the scanning Kelvin probe (SKP) has shown to be a high-resolution technique for *in*-situ assessment of the interfacial stability for both coatings and adhesives, by measuring the corrosion potential of the buried electrode at the metal/polymer interface [8–11]. Khun and Frankel used the SKP to study the effect of surface roughness and texture on the kinetics of cathodic delamination of epoxy coated steel [12]. They showed that the delamination rate of coatings dramatically decreased by gradually increasing the surface roughness from 11 to 305 nm. Similar to Zielecki et al. and earlier work by Watts and Castle they conclude that the surface roughness effect can be assigned to the increased interfacial surface area and the associated increased number of interactions across the interface. Rudawska too studied the effect of mechanical treatment on surface roughness, but concluded that the geometrical structure of the surface, which determines the adhesive's penetration capability, is of more significant importance than the surface area [13]. It is clear from the aforementioned studies that there is some debate regarding the effect of surface roughness, without even taking synergistic effects of chemistry into account.

As well as the surface roughness, many studies have been devoted to solely study the effect of surface chemistry on the adhesion between polymers and steel. Wielant et al. found that the adhesion of epoxy-amide films on polished steel was highest for highly hydroxylated surfaces because of the formation of relatively strong Brønsted acid–base interactions [14]. Using a combination of infrared-, electrochemical impedance spectroscopy and SKP Sababi et al. studied the effect of zirconium based conversion treatments on the interfacial bonding properties of polished epoxy coated steel [15]. They found that changing the surface chemistry has a profound effect on both the initial adhesion strength and durability of adhesion through improved interactions and chemical stability at the interface. Likewise, organosilane-based surface pre-treatments have been known already for some decades to promote adhesion through the promotion of covalent bonding across the interface [16,17].

According to our knowledge, no study has been dedicated to systematically study the effect of individual surface properties of steel on both the initial adhesion and its durability. Hence, the main goal of this work is to obtain a better fundamental understanding about the

mechanisms and phenomena responsible for strong initial adhesion and the durability in corrosive environment. Therefore, we studied this by creating distinctively different surfaces in order to discriminate between the contributions of chemical and mechanical bonding mechanisms. Various pre-treatments were used to alter the surface textural and chemical properties and surfaces were characterized prior to assessment by mechanical testing, exposure test and scanning Kelvin probe. The combination of these techniques provides complementary information about the adhesive bond failure mechanism and interfacial delamination kinetics.

2. Experimental

2.1. Materials

A S690QL hot-rolled, high-strength low-alloy steel (C ≤ 0.1 wt%, Mn ≤ 1.80 wt%, Si ≤ 0.80 wt%, Ni ≤ 2.0 wt%, S ≤ 0.010 wt%, Cr ≤ 1.5 wt%, balance Fe) was used as substrate. The adhesive studied is a two-part epoxy system, Araldite® 2015 from Huntsman Advanced Materials (Switzerland) GmbH. This is a DGEBA based epoxy with an amine hardener. Mixing of the two components was done using an adhesive applicator gun with a mixing nozzle in a 1:1 ratio. Curing was performed with the recommended cycle of 24 h at room temperature, followed by a post-cure of 1 h at 80 °C to ensure full curing.

2.2. Surface preparation

All as-received steel samples were ultrasonically cleaned for 5 min in acetone, using an Emag Emmi 20HC ultrasonic cleaner, and subsequently rinsed for 10 s with isopropyl alcohol to remove any surface contaminants. After cleaning, the surfaces were subjected to a range of mechanical and chemical pre-treatments to create distinctively different surfaces. Fig. 1 provides a schematic overview of the different surface pre-treatments and their corresponding effect on the surface properties.

2.2.1. Industrial reference
The industrial reference, grit blasting, was prepared on cleaned specimens that were then pre-treated using a dry grit blasting machine at a pressure of 3.5 bar at a distance of 20 cm and an angle of approximately 45° with white alumina particles (mesh 180–230). Since specimens with a range of dimensions are used, blasting time varies per specimen type. Passing speed of the nozzle of the blasting machine was manually kept at a continuous speed. After blasting, residual grit particles and dust were removed by compressed air.

2.2.2. Mechanical surface treatment
Different grades of surface roughness were created by mechanical abrasion of the surface with an automated grinding- and polishing machine (Struers Rotopol 31/Rotoforce 4, Struers A/S). Grinding was conducted at a paper disc rotation speed of 150 rpm and a sample rotation speed of 40 rpm at a pressure of 0.5 MPa. Different SiC paper grades were used: 80-, 180- and 320-grit.

2.2.3. Chemical surface treatment
To eliminate the effect of surface texture and the associated mechanical interlocking on different chemically treated samples, steel substrates were polished to remove any textural features. The samples were abraded with abrasive SiC paper up to 2000-grit and subsequently polished using a diamond suspension paste of 3 μm and 1 μm particles. After mechanical abrasion and polishing, the specimens were ultrasonically cleaned in acetone for 5 min, rinsed with isopropyl alcohol for 20 s and dried with compressed air. ***Alkaline treatment*** was performed by immersion in a 1 M KOH solution for 10 min at 60 °C under continuous stirring of the solution at 500 rpm using a magnetic stirring plate. Specimens were subsequently rinsed for 10 s with DI water and dried with compressed air. This procedure was selected based on the work of
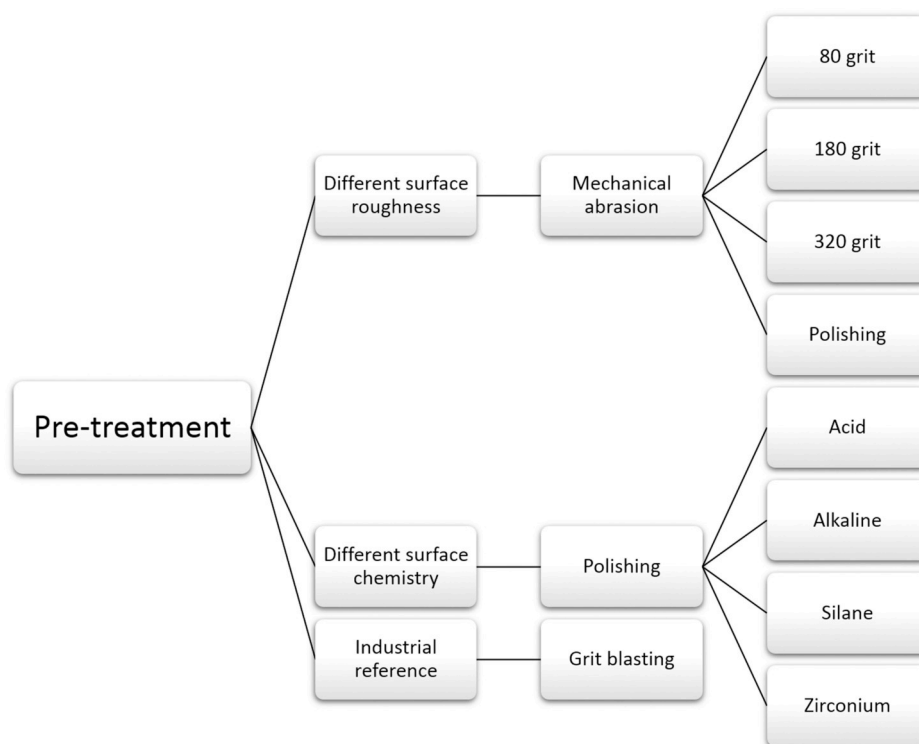
Fig. 1. Schematic overview of applied surface pre-treatments.

Wielant et al. [18], who have shown to form alkaline oxides with a relatively high surface hydroxyl fraction through this treatment. The ***acid treatment*** was applied by immersion of the steel samples in a mixture of 5 vol% nitric- and 30 vol% phosphoric acid, based on the method of Kozma and Olefjord [19]. Specimens were subsequently rinsed for 10 s with DI water and dried with compressed air. The ***silane*** used in this study is γ-glycidoxypropyltrimethoxysilane (γ-GPS), which has an epoxy functional group at the end of the organic chain. γ-GPS is selected for its compatibility with the adhesive system due to this epoxy group, thereby promoting the formation of covalent bonding across the interface [20–22]. Treatment conditions, such as hydrolysis time, pH, hydrolysis solvents and curing time were adapted from the work by Li et al. [17]. The pH of a 10 vol% γ-GPS solution in an 8:1 ratio DI water/methanol mixture was adjusted to 5.5, using acetic acid, and was hydrolyzed for 48 h at room temperature under continuous stirring. In order to improve the metal hydroxyl density, the steel surface was treated with a 1 M KOH solution at 60 °C for 10 min prior to silane film deposition. Silane film deposition was performed by immersion of the steel sample in the hydrolyzed silane solution for 10–20 s. After deposition, the excess silane solution was removed from the surface by a flow of nitrogen gas and the samples were cured in an oven at 150 °C for 1 h under air atmosphere. Samples were left for 15–20 min to cool down to room temperature before the application of the adhesive.

The procedure for the ***zirconium conversion treatment*** of the steel surfaces was adopted from Asemani et al. [23]. Prior to the deposition of the conversion coating, the steel samples were immersed for 10 min in 1 M KOH at 60 °C to improve the metal hydroxyl density and subsequently rinsed with deionized (DI) water for 10 s and dried with compressed air. The conversion solution was a 0.01 M hexafluorozirconic-acid solution consisting of 50 wt% H_2ZrF_6 (purchased from Sigma-Aldrich) and DI water. The pH was adjusted to 4.5 using 1 M KOH and 1 M HCl. Samples were immersed for 90 s at 30 °C, under continuous stirring at 180 rpm. After conversion coating deposition, the samples were rinsed with DI water for 10 s and dried under a flow of nitrogen.

2.3. Surface analysis

The effect of the different surface pre-treatments on the physicochemical properties of the steel substrate was studied using various surface analysis techniques. Surface morphology, texture and roughness were measured using scanning electron microscopy (SEM), atomic force microscopy (AFM) and confocal laser scanning microscopy (CLSM). Energy dispersive Spectroscopic (EDS) analysis was used to determine the surface chemistry.

2.3.1. Scanning electron microscopy (SEM)
SEM was done using a JEOL IT100 Scanning Electron Microscope (SEM), coupled with an energy dispersive spectrometry (EDS) analyzer. Images and spectra of pre-treated surfaces were obtained at a magnification of one-thousand at an acceleration voltage of 20 kV and processed with corresponding InTouchScope™ software.

2.3.2. Confocal laser scanning microscopy (CLSM)
An Olympus LEXT OLS3100 system was used to acquire confocal scanning laser microscopic images (CLSM) of the highly textured samples i.e. mechanically abraded, grit blasted and etched samples. The magnification was set to 100× and roughness measurements were performed on an area of 90 by 90 μm (*xy* plane).

2.3.3. Atomic force microscopy (AFM)
AFM measurements were conducted on the samples with low surface texture, using a Bruker Dimension Edge™ in tapping mode with an antimony (n) doped silicon tip. The measurements were conducted with a pixel resolution of 256 × 256 and scan rate of 0.6 Hz. Nanodrive v8.05 software was used for conducting experiments. Multiple locations on the surfaces were scanned covering an area of 30 by 30 μm (*xy* plane).

The surface roughness was determined from the CLSM and AFM data using ISO 25178 in two ways: (i) from the different surface parameters and (ii) from the ratio of the 3-dimensional area of the imaged sample to the planar (projected) area which gave the relative surface area and an expression for the area contributed by the texture [24]. Each value is an

average of four measurements, taken at random locations on the surface. All values have been determined using Gwyddion software v2.50 for scanning probe data analysis.

2.4. Adhesion testing

All substrates were bonded or coated within a few minutes after surface pre-treatment to avoid superficial changes e.g. excessive oxidation or adventitious contamination. Table 1 presents the bonded joint- and open-specimen geometries tested in this study and their dimensions.

2.4.1. Single-lap joint (SLJ) shear test

Single-lap joint (SLJ) shear tests were performed to analyze the effect of the different surface treatments on the initial bond strength between the adhesive and the pre-treated steel. The SLJ shear test is a widely used industrial test [25–27], and the current geometry is based on the standard geometry defined in ASTM-standard D1002. In order to assure the final geometry of the joint specimens, a mould was used to align the specimens, control the bondline thickness and provide uniform pressure across the joints. Tabs were glued at the specimens' ends for a correct alignment in the testing machine. The initial bond strength was calculated as the failure load divided by the fracture surface area. Five joints of each specimen type were tested in tensile load with a Zwick® Z010 (Zwick Roell AG, Germany) electro-mechanical testing machine with a 10-kN load cell, at room temperature and under displacement control (1.3 mm/min).

2.4.2. Static wedge test (SWT)

In the geometry of the static wedge test, the adhesive joint is subjected to peel loading [28]. The SWT is therefore used in this study to assess the durability of the interface and the adhesive joints in peel loading mode in a saline solution. The wedge test was originally designed for aluminum substrates with the standard geometry described in ASTM standard D3762. Tests were performed as specified in this standard, with the specimen geometries adapted to the mechanical properties of the steel substrate. Assembly of the specimens consisted of bonding individual pairs of steel coupons, with dimensions of $150 \times 25.4 \times 1.9$ mm. Bondline thickness was controlled to be 0.7 ± 0.05 mm, by inserting steel shims at the tip and tail prior to curing. After curing of the adhesive these spacers were removed. A mould was used to assure correct alignment of the specimens and uniform pressure across the entire length of the joint assemblies [29]. After curing, steel wedges were inserted into the bonded joints and the samples were conditioned for 1 h before being immersed for 700 h in a 3.5 wt% sodium chloride solution at room temperature. For the final geometry, see Fig. 2. As for the single-lap joint specimens, five joints of each specimen type were tested in the static wedge test.

Crack lengths were measured prior to immersion and at regular time intervals up to 700 h. Based on the measured crack lengths and specimen dimensions, the fracture toughness values, G_I (J m^{-2}), were calculated using Eq. (1)
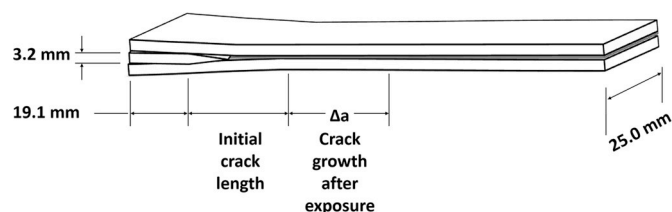

Fig. 2. Wedge joint geometry.

$$G_I = \frac{Ed^2h^3}{16} \frac{\left[3(a + 0.6h)^2 + h^2\right]}{\left[(a + 0.6h)^3 + ah^2\right]^2} \tag{1}$$

where E is the adherend's Young's modulus (210 GPa), d is the crack opening displacement, defined as the thickness of the wedge minus the bondline thickness, h is the adherend thickness, and a is the measured crack length.

2.4.3. Scanning Kelvin probe (SKP)

The SKP delamination measurements were performed on the steel substrate coated with a thin film of adhesive.

The sample preparation method was adopted from Warren et al. [30]. The dimensions of the steel specimens and adhesive film thickness are listed in Table 1. A 15 by 30 mm strip of PTFE tape was placed near the edge of the sample. Two parallel strips of adhesive tape were applied perpendicular to the PTFE tape, leaving an area of 30 by 15 mm of the metallic substrate in the middle. The parallel strips act as spacers to control the thickness of the adhesive film to be 50 ± 5 μm. The adhesive was applied onto the metallic surface and spread with a polished steel rod, leaving a smooth film. The PTFE tape was then lifted in order to create an area of bare substrate which acts as an artificial defect. A Permatex® 80022 silicone gasket was applied to create a reservoir which could contain over 3 mL of aqueous sodium chloride solution during the experiment.

The sample was placed in the humidity chamber of the Kelvin probe instrument (SKP5050) for at least 12 h and allowed to equilibrate at a relative humidity of 93%. After equilibrating, 3.5 wt% of sodium chloride solution was added to the defect to initiate delamination. A Ni/Cr probe was used with a 500 μm circular flat end. The probe was scanned over the adhesive film along a 25-mm line away from the defect towards the intact area. The probe was set to vibrate at a 61 Hz frequency amplitude of 50 μm, with a tip-to-sample separation of 75 μm.

Prior to each SKP experiment, the probe was calibrated in order to avoid a potential shift of the probe. A Cu/CuSO$_4$ reference electrode was used and the measured potential was converted to the standard hydrogen electrode potential (0.316 V vs SHE). The calibration procedure is explained in detail elsewhere [31]. All SKP delamination measurements were performed at room temperature and controlled relative humidity of 93%.

3. Results and discussion

3.1. Surface characterization

The direct effect of surface treatments on the surface texture was observed by SEM. Representative SEM images of pre-treated surfaces are given in Fig. 3. Fig. 3(a-c) shows the results after mechanical abrasion of the steel surface. A clear scratchy directional pattern with small pores can be observed with finer scratches and pores corresponding to higher grit grades of the abrasive paper.

Fig. 3(d) shows the surface of the sample after polishing. It is evident, compared to the images of the abraded surfaces, that the surface shows no sign of textural or morphological features and that the microstructural features of the steel become visible. The morphology of the surface

Table 1
Specimen dimensions of single-lap joint, wedge joint and scanning Kelvin probe test.

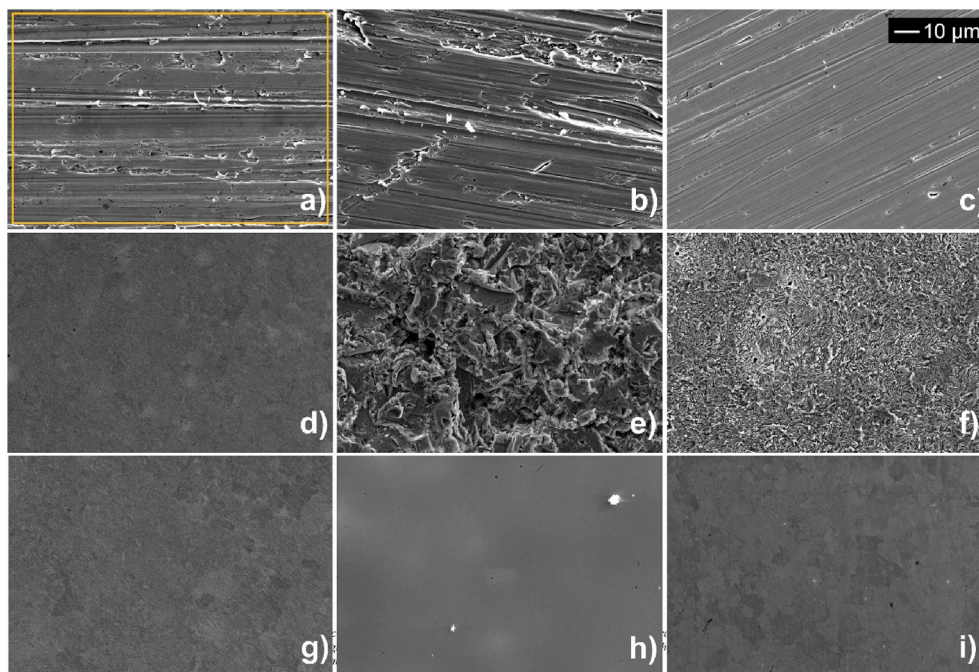| Type	Substrate thickness (mm)	Overlap/ width (mm)	Adhesive thickness (μm)	Loading mode
Single-lap joint	4.0	12.7/25.0	200 ± 40	Shear/ Mode II
Wedge test joint	1.9	131.9/25.0	700 ± 50	Opening/ Mode I
Scanning Kelvin Probe	4.0	n.a./ 15.0×30.0	50 ± 8	None

Fig. 3. Surface images from SEM analysis for different surfaces after mechanical abrasion with different grades of SiC paper (a) 80-grit, (b) 180-grit, (c) 320-grit, (d) polishing, (e) grit blasting, (f) nitric-phosphoric acid etching, (g) alkaline treatment, (h) silane and (i) zirconium conversion treatment.

produced by grit blasting is shown in Fig. 3(e). The surface shows a distributed roughness profile with an even distribution of deep and more shallow pores or craters, which are a result of the material removal by indentation of the blast grits [32]. The image of the surface treated by acid etching after polishing is shown in Fig. 3(f). Acid treatment has resulted in the formation of microscopic lamellae creating a furrowed morphology with fine scale micropores of which the scale is much finer

compared to the grit blasted surface. It is clear from the SEM images that both grit blasting and acid etching results in a morphology with a high degree of microroughness. Both pre-treatments create a higher degree of texturing compared to the mechanically abraded surfaces, with a significantly finer structure in the case of etching that indicates an enlarged surface area. Surfaces after the alkaline-, silane- and zirconium conversion treatments are shown in Fig. 3(g–i). The alkaline treated
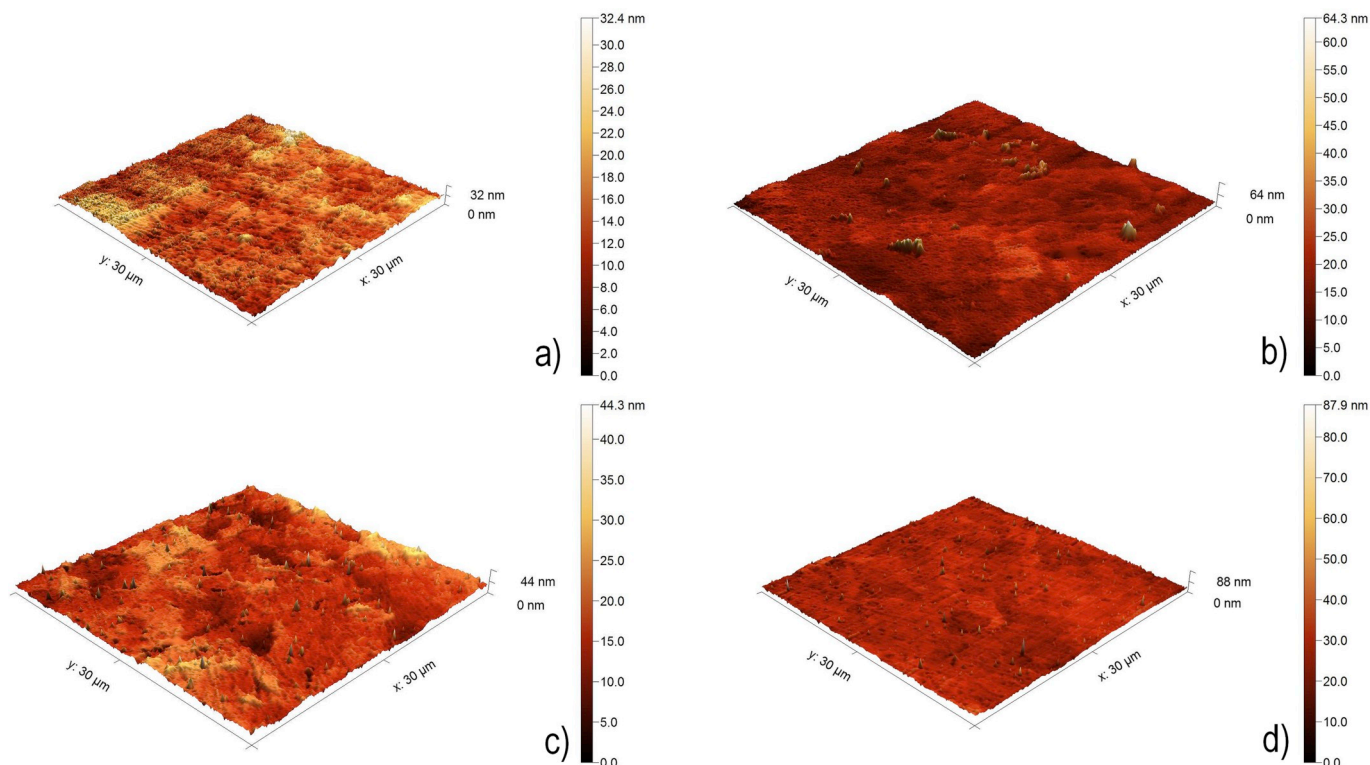

Fig. 4. AFM images of surfaces after (a) polishing (b) silane application (c) alkaline treatment and (d) zirconium conversion treatment.

samples show no morphological changes compared to the polished surface in Fig. 3(d). The silane treatment has considerably altered the surface morphology of the steel surface. Fig. 3(h) shows a homogeneous film on the surface with local deposition of clustered silane oligomers (white spots). Fig. 3(i) displays the surface of the steel after the zirconium conversion treatment. The treatment emphasizes the microstructural features of the steel and some small zirconium oxide particles have aggregated on the surface, indicated by the white spots in Fig. 3(i).

AFM analysis of the corresponding surface topography of polished and chemically pre-treated surfaces are shown in Fig. 4. AFM images confirm that polishing the steel samples has resulted in the removal of all surface texture and morphological features, with a maximum peak to valley height of only 32.4 nm. Some larger nodes and peaks are observed on the surfaces after silane and zirconium treatments, but these are attributed to the formation of zirconium oxide/hydroxide particles and agglomerates in the deposited silane film. Like zirconium and silane, alkaline treatment has not induced any texturing or significant morphological changes of the surface. Albeit the presence of minor surface features, no significant roughening or texturing is introduced by these chemical treatments.

In order to describe and quantify the surface in terms of roughness, several surface roughness parameters can be used. The most common of which is the arithmetic mean height, S_a.

$$S_a = \int \int_a |Z(x,y)|(dx)dy \tag{2}$$

This parameter alone is not adequate enough to assess the surface topography, as different surface profiles can exhibit the same or similar S_a values [33]. If the varying heights along a profile of a (rough) surface are considered as a distribution, it is possible to gauge whether a profile is skewed towards broad peaks and spike-like valleys, or towards broad valleys and spike-like peaks. The parameter used to give this information is skewness, or S_{sk} [33].

$$S_{sk} = \frac{1}{S_q^3} \int \int_a (Z(x,y))^3 (dx)dy \tag{3}$$

where S_q is the root mean square roughness. The skewness shows the degree of asymmetry of the surface about the mean plane. $S_{sk}<0$ indicates a height distribution above the mean plane, so a flat surface with holes and $S_{sk}>0$ denoted a height distribution below the mean plane, so a flat surface with peaks, where values $>|1|$ may indicate extreme holes or peaks on the surface. Combined with S_a, the skewness parameter can be used to describe the surface profile. The third roughness parameter used to describe the roughness, or texture of a surface is the developed interfacial area ratio, S_{dr}.

$$S_{dr} = \frac{1}{A}\left[\iint_A \left(\sqrt{\left[1 + \left(\frac{\partial z(x,y)}{\partial x} \right)^2 + \left(\frac{\partial z(x,y)}{\partial y} \right)^2 \right]} - 1 \right) dxdy \right] \tag{4}$$

S_{dr} expresses the additional percentage of the scanned surface area, contributed by the texture of the surface, also referred to as the relative surface area increase. Combining these three parameters enables to quantitatively assess the topography of the surface.

The roughness, skewness and interfacial area ratio values are determined by processing of the AFM- and CLSM data for the different surface treatments and are presented in Table 2.

All polished surfaces, before and after chemical treatments, have very similar roughness values in the low nanometer range (2.6–3.6 nm). The polished surface exhibits the lowest S_a value of 2.5 ± 0.57 nm and the skewness of 0.39 indicates a height distribution below the mean on the surface, caused by small peaks on the surface. The 0.0% developed interfacial area ratio confirms that due to the absence of surface texture, there is no relative increase in the surface area. Subsequent chemical treatment of the polished surfaces shows to induce no significant

Table 2
Average surface roughness (S_a), skewness (S_{sk}) and the developed interfacial area ratio (S_{dr}) for different pre-treatments.

Pre-treatment	S_a (nm)	S_{sk}	S_{dr} (%)	Method
#80 grit	380 ± 26	-0.90 ± 0.08	19.4 ± 3.2	CLSM
#180 grit	210 ± 23	-0.76 ± 0.09	14.5 ± 1.2	CLSM
#320 grit	180 ± 17	-0.28 ± 0.03	11.6 ± 1.6	CLSM
Polished	7.1 ± 0.4	0.02 ± 0.00	0.0 ± 0.0	CLSM
	2.5 ± 0.6	0.39 ± 0.10	0.0 ± 0.0	AFM
Grit blasted	1020 ± 229	-1.29 ± 0.09	48.6 ± 4.9	CLSM
Acid	294 ± 19	0.31 ± 0.02	39.4 ± 3.9	CLSM
	220 ± 5	0.47 ± 0.14	23.7 ± 1.2	AFM
Alkaline	2.9 ± 0.1	0.66 ± 0.28	0.0 ± 0.0	AFM
γ-GPS	3.6 ± 0.6	1.73 ± 0.36	0.0 ± 0.0	AFM
ZrCC	2.6 ± 0.2	1.81 ± 0.26	0.0 ± 0.0	AFM

alteration of the arithmetic surface roughness, as can be seen by the S_a values for the zirconium (2.6 ± 0.22), alkaline (2.9 ± 0.11) and silane treated specimens (3.6 ± 0.59). The high positive skewness values for the zirconium (1.81 ± 0.26) and silane (1.73 ± 0.36) treated specimens confirms the presence of sharp peaks on the surface, which are observed in the AFM images in Fig. 4. No significant increase in the relative surface area can be observed for all of these chemical treatments, despite the presence of local peaks on the silane- and zirconium treated surfaces.

The mechanically abraded surfaces have much higher roughness values, with S_a two orders of magnitude higher than the polished samples (380, 210 and 180 nm). S_a values increase with coarser abrasive paper and the skewness for all abraded samples is negative, indicating the presence of more valleys in the surface than peaks or that the valleys in the surface are sharper. The latter correlates with the scratchy pattern observed earlier by SEM caused by the superficial removal of material during abrasion. The relative surface area increase follows the same trend as the aforementioned S_a values (19.4, 14.5 and 11.6% respectively), with higher surface area increase corresponding to rougher surfaces.

The acid-treated surface roughness is in the same order of magnitude as the coarsely abraded surfaces, with an average roughness of 294 ± 19.3 nm. The fine porous morphology of the surface creates a high developed interfacial area ratio, with an increased surface area of 23.7–39.4%. The low positive skewness of the acid treated surface describes the fine-scaled microporous structure etched into the surface. Like the acid treatment, the grit blasted surface demonstrates the highest developed interfacial area of 48.6%, created by the coarser porous structure at the surface. The large negative skewness (-1.29) confirms the micro-cutting and deep indentation of the surface by the abrasive grits. The grit blasted specimens exhibit the highest S_a of over 1 μm.

EDS analysis was used to evaluate alterations in surface chemistry after the different pre-treatments. Fig. 5 shows the EDS spectra obtained by area scans of the SEM images in Fig. 3. All spectra show high signal counts for iron and for manganese, the main alloying element of the steel. Comparing the chemical composition of the abraded specimens to the polished sample shows the presence of silicon, due to the remaining presence of abrasive particles embedded in the steel surface. The spectrum of the grit blasted specimens shows high signals for both aluminum and silicon caused by the indentation and incorporation of grit particles into the surface. The acid and alkaline treated samples both show a chemical composition similar to that of the polished sample. The high silicon signal for the silane treated surfaces confirms the deposition of a silane layer, observed as a homogeneous film in the SEM and AFM analysis. For the zirconium treated specimen clear traces of zirconium and fluoride are detected in the spectrum. The lower intensities for zirconium and fluoride, compared to the silicon signal in the silane treated sample, can be explained by the thickness of the two conversion layers, which normally is an order of magnitude thinner in the case of zirconium treatment.
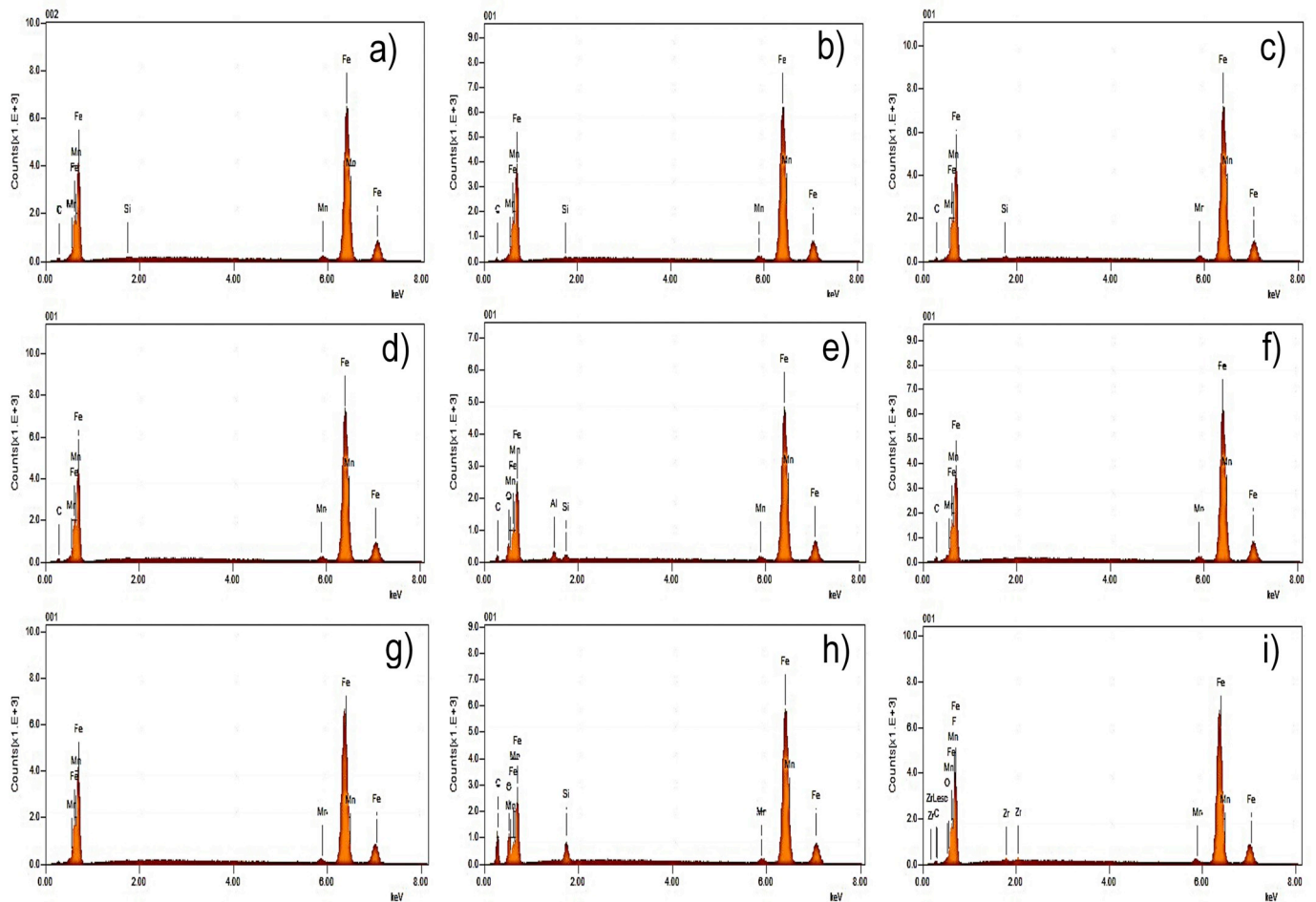
Fig. 5. EDS analysis from the steel surfaces depicted in Fig. 3 after mechanical abrasion with different grades of SiC paper (a) 80-grit, (b) 180-grit, (c) 320-grit, (d) polishing, (e) grit blasting, (f) nitric-phosphoric acid etching, (g) alkaline treatment, (h) silane and (i) zirconium conversion treatment.

3.2. Mechanical testing

3.2.1. Single-lap joint (SLJ) shear test

The results of the shear strength test for adhesively bonded lap joints, after the different pre-treatments, are presented in Fig. 6. It is clear from the figure that the ultimate shear strength of the joint is highly dependent on the type of surface treatment.

The grit blasted samples exhibit the highest shear strength of all measured samples, with an average shear strength value of 20.7 MPa. The second highest shear strength is obtained by the acid treatment. Samples after roughening of the surface by mechanical abrasion show relatively high shear strength values, ranging from ~15 to 18 MPa. Further refining of the surface by polishing and creating a mirror-like appearance has a deleterious effect on the shear strength, which drops to 12.9 MPa. Alkaline treatment of the polished surface even further diminishes the shear strength and this treatment shows the lowest obtained shear stress value of 9.6 MPa. Subsequent conversion layer application on alkaline cleaned surfaces by either silane or zirconium treatment shows a significant increase of the shear strength, with silane treated samples reaching similar values as the 80 grit abraded samples.

It is clear from Fig. 6 that the textured surfaces exhibit the highest shear strengths in the SLJ test, in which the highest values are obtained by the acid treated and grit blasted surfaces and a general downward trend can be seen in the performance of the abraded samples, where higher grit SiC paper lead to lower shear strengths. Fig. 7 plots the shear strength vs. the roughness of the mechanically abraded surfaces, expressed by the arithmetic mean height (Fig. 7 (a)) and the developed
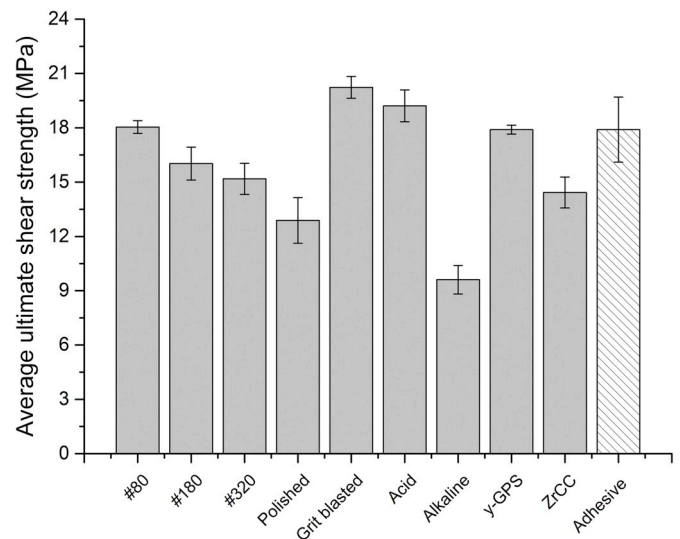

Fig. 6. Average ultimate shear strength of single-lap joint specimens for the range of surface treatments. Intrinsic strength of the adhesive obtained from da Silva et al. [25] added as comparison.

interfacial area ratio (Fig. 7 (b)). It is clear from the figures that the roughness has a profound effect on the adhesion and that for both roughness parameters a similar correlation with the shear strength can
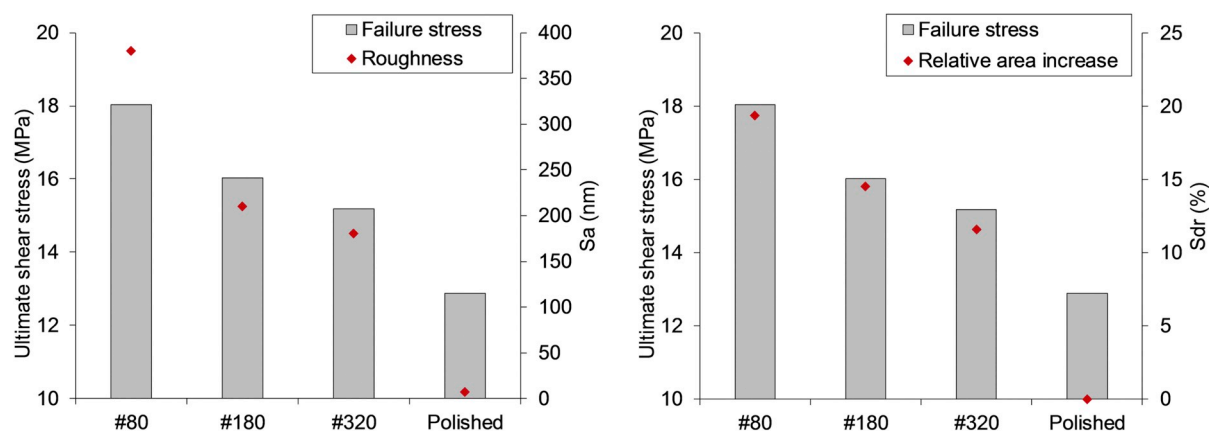
Fig. 7. Average ultimate shear strength of single-lap joint specimens with mechanical treatments versus (a) arithmetic mean height, S_a and (b) developed interfacial area ratio, S_{dr}.

be found. From the SEM analysis and the skewness, determined by CLSM, it was found that the abraded surfaces exhibit a sharp scratchy surface texture. Such scratches provide a larger surface area for bonding with the adhesive and the possibility for the adhesive to flow into the scratches, but no interlocking inside these surface features. Observing the similar trend for both average roughness and the developed interfacial area, proves that the enhanced adhesion as a result of mechanical abrasion can be primarily attributed to the increased surface area induced by the roughening and not to mechanical interlocking.

Acid treatment results in the second highest shear strength, superior to all mechanically abraded samples, despite having similar arithmetic roughness values. This demonstrates the effect of a highly textured surface morphology on bonding strength, which can be attributed to several mechanisms. The microporous morphology of the surface creates a large increase in the interfacial area ratio, thereby significantly increasing the number of bonding sites at the interface between the adhesive and adherend. Apart from this, the highly microporous surface allows the adhesive to penetrate into the surface features and interlock by curing inside the pores. Besides the effect of increased surface area and mechanical interlocking, the acid treatment could also alter the type and number of interactions between the adhesive and the substrate. According to Pohl et al. acid treatments can lower the hydroxyl fraction at the surface, thereby promoting strong Lewis acid-base interactions between the acidic metal and the basic amino groups in the epoxy adhesive [34]. Since no traces of nitrogen of phosphor were found in the EDS, a possible contribution to the improved adhesion by incorporated phosphates or nitrates can be excluded.

Like acid treatment, grit blasting of the surface creates specimens with superior shear strengths, reaching values that are well above the intrinsic shear strength of the adhesive of 17.9 MPa (indicated in Fig. 6) [25]. The strength of the grit blasted samples could be linked to the high average roughness of the surface, which is an order of magnitude higher than the abraded and acid treated surfaces, and to the increased developed interfacial area. An enhanced effect of mechanical interlocking due to the deeper penetration of the thixotropic adhesive into the coarser porous texture of the surface could also be a key parameter on this improved adhesion.

Considering the values of the silane and zirconium treated samples there is a significant increase in the shear strength compared to the polished sample, with a relative increase of over 5 MPa in the case of silane treatment. Despite the absence of surface texture, the silane treated samples show a shear strength in the same order as the samples with a high degrees of surface texturing; grit blasted, acid and 80-grit abraded. This enhanced adhesive strength can be directly assigned to the covalent bonding mechanism induced by the deposited silanes with active epoxy groups [35]. The improved interfacial adhesion after zirconium treatment could be related to the type of interfacial acid-base

interactions and improved surface hydroxyl fraction, as was proposed for other metals [36]. On the contrary no enhanced effect on the adhesion strength is found for the alkaline treated surfaces, which according to earlier studies leads to increased hydroxyl fractions [37]. This suggests that not merely the increased hydroxyl fraction contributes to the increased adhesion strength in the case of zirconium treatment.

The main failure mechanisms of adhesive joints can be generally divided into three modes: failure at the adhesive-adherend interface (adhesive failure); intrinsic failure of the adhesive (cohesive failure); and a mixed mode with both cohesive and adhesive failure. Here, the strength of adhesion at the adhesive-adherend interface is a dominant parameter in the failure mechanism [38]. In Fig. 8 the different failure modes and their corresponding pre-treatments are shown. In the case of our test specimens we see a clear trend in the different modes of failure of the specimens. All samples with average shear strength values higher than 18 MPa exhibit cohesive failure as the dominant failure mode. This includes grit blasting, acid treated and the 80-grit abraded samples and can be directly attributed to the exceeding of the shear stress above the intrinsic shear strength of the adhesive. The mid-range specimens; silane, zirconium and the lower grit abraded surfaces exhibit a mixed failure mode. The polished samples and the alkaline treated polished samples show an adhesive mode of failure, as indicated by the re-appearance of the mirror-polished surface after fracture.

From the single lap joint results it becomes evident that not only roughening of the surface and the corresponding triggering of mechanical interlocking and/or increasing the reactive surface area is able to cause a significant increase in shear strength. As expected, increasingly rough surfaces lead to stronger joints, with the roughest abraded surface leading to highest shear strength values. Nevertheless, higher shear strength values are obtained for polished and subsequently silane-treated specimens, indicating the importance of surface chemistry and the contribution from covalent bonds. In the absence of enhanced physical or chemical bonding, adhesion at the interface depends merely on the intimate contact between the adhesive and the steel substrate.

3.2.2. Static wedge test

The wedge test has proven to be highly reliable in determining and predicting the environmental durability of adherend surface preparations [28,39]. Thanks to the insertion of a wedge into the bonded assembly, the interface is subjected to high tensile stresses. This method simulates in a qualitative manner the forces and effects on an adhesive bonded joint at the metal-adhesive interface. The initial crack created prior to exposure arrests when the local stresses at the crack-tip become lower than the intrinsic ultimate tensile strength of the adhesive. The residual stresses are therefore focused on the interface, making it the locus of failure upon degradation of the interface.

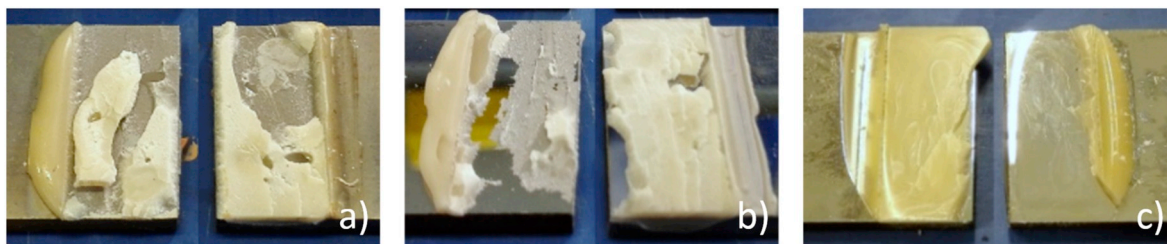Fig. 9 displays the measured crack length of the static wedge test

Fig. 8. Typical images of fractured surfaces illustrating (a) cohesive failure after nitric-phosphoric acid etching (b) mixed mode failure after silane treatment and (c) adhesive failure after polishing.

specimens during full immersion in 3.5 wt% NaCl solution and their relative crack growth. Similar trends can be observed for both graphs, with the lowest values being recorded for the grit blasted samples. Right after insertion of the wedge, significant differences can be observed in initial crack lengths, with values ranging from approximately 30 mm for grit blasted samples to around 50 mm for the polished samples. During the initial hour of exposure, a rapid increase of the crack length can be observed for mechanically abraded samples and the polished sample. Grit blasting, silane and zirconium show a moderate increase in crack lengths. This trend in lower crack length (grit blasting < silane < zirconium) can be observed during the rest of the exposure time. The 80-grit mechanically abraded sample shows the fourth best performance in terms of crack length. Noticeable is the larger crack growth during the long-term exposure stage (200–700 h). For the top three samples in Fig. 9 the propagation of the crack length appears to accelerate whereas the lower four show similar growth rates over time.

Fig. 10 shows the corresponding plots of mode I fracture toughness, computed from the measured crack length using Eq. (1), versus the exposure time. The initial values of the fracture toughness already show a large scatter. Noticeable is the high value of the silane treated samples at t = 0.1 h, followed by 80 grit and the grit blasted surface. These pre-treatments also resulted in the highest ultimate shear strength, obtained from the shear test of the single lap joints.

During the initial hours of exposure, we see a similar trend for most samples, except the zirconium-treated and grit blasted surface. The latter shows a gradual decrease in fracture toughness, indicating the propagation of the crack within the adhesive. This is confirmed by optical evaluation. The residual samples show a rapid decrease in fracture toughness to values around $100 \, J/m^2$. After an exposure time of approximately 4 h we see a similar drop in the case of the zirconium treated samples, indicating the transition from cohesive to an adhesive
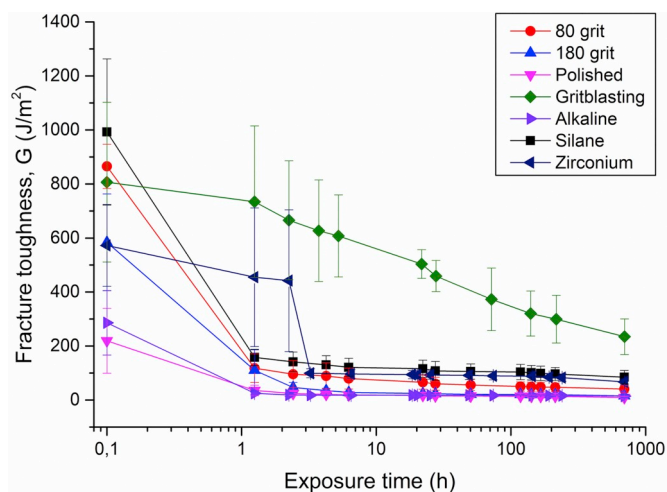

Fig. 10. Fracture toughness vs exposure time.

failure mode.

In the case of the grit blasted specimens, there is a gradual decrease in the fracture toughness, which is reaching a final value of approximately $234 \, J/m^2$. Post-exposure evaluation shows a mixed mode of failure, interfacial and near-interfacial failure. This is indicated by signs of exposed and corroded surfaces as well as residual adhesive after opening of the joint.

After the initial drop, the residual samples (all apart from grit blasted) show a gradual decrease of the fracture toughness reaching final values of 9, 15 and $40 \, J/m^2$ for the polished, 180 grit and 80 grit,
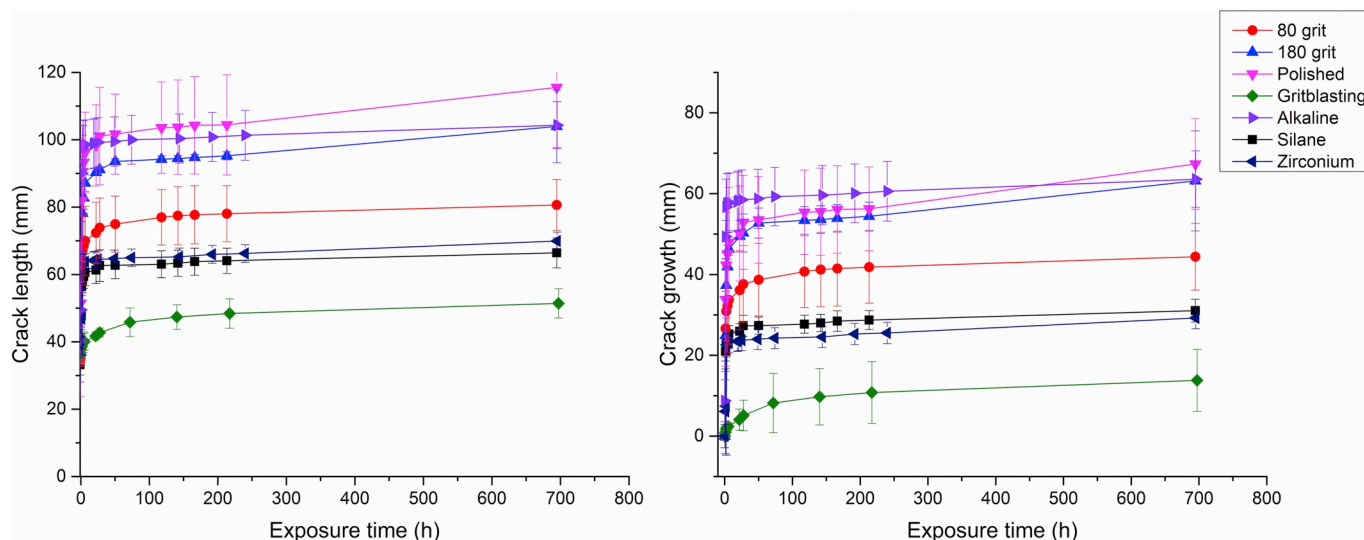

Fig. 9. (a) crack length vs exposure time (b) crack growth vs exposure time.

respectively and 67 and 85 J/m^2 for the polished samples with zirconium and silane treatment, respectively. The chemically treated samples show a residual fracture toughness that is 7–9 times higher relative to the polished samples. This clearly demonstrates the benefit of improved intermolecular and interatomic bonding across the interface, promoted by the two chemical surface pre-treatments, on the durability of the interfacial adhesion. The performance of the grit blasted samples compared to the abraded samples, demonstrates ones more that the improved adhesion and durability cannot be merely explained by the increased roughness of the surface. It is clear that changes in physical, chemical and morphological properties have a significant contribution to the joint performance in terms of both dry and wet adhesion. This corresponds to the work of Harris et al. who investigated the effect of grit-blasting on adhesion [40].

3.3. Scanning Kelvin probe (SKP)

The SKP measurements were performed to study the effect of the different surface treatments on the corrosive delamination kinetics of the epoxy film from the steel substrate. In the experimental setup for the SKP, a 50-μm film of adhesive is applied on the steel surface. The interface was then exposed by the creation of an artificial defect and electrolyte reservoir. The scanning Kelvin probe is then used to assess the effect of the different treatments on the delamination kinetics of the adhesive from the steel substrate. With the kelvin probe vibrating over the polymer coated surface, the corrosion potential of the substrate can be measured. The distribution of the corrosion potential underneath the film provide information on delamination kinetics and mechanisms [41, 42].

In this setup, the system is in an unloaded condition during exposure, therefore providing merely information on the resistance to corrosion-driven delamination at the interface.

For these measurements three different treatments have been selected; polishing, 80 grit mechanical abrasion and silane treatment. The polished surface has been selected for its poor performance in the mechanical test and due to the absence of both roughness and altered surface chemistry. The two latter treatments have been selected based on their superior performance in terms of both dry- and wet adhesion in the SLJ and SWT test.

Fig. 11 illustrates the measured potential profiles as a function of time for the polished and the silane-treated specimens. All three SKP potential profiles are characterized by a sharp transition between two levels, corresponding to the defect potential (around −400 mV$_{SHE}$) and the high potential of the intact bonded region (around 0 mV$_{SHE}$). The location of this transition is designated as the location of the delamination front, as described in pioneering work by Leng et al. [43]. The potential of the defect region is around −400 mV$_{SHE}$, which corresponds to the corrosion potential of the steel substrate. The potential of the intact region fluctuates around 0 mV$_{SHE}$. Looking at the position of the transition region, it is clear from Fig. 11(a) that the delamination front for the polished sample is moving rapidly over time, covering a distance of over 22 mm in 24 h. The silane treated surface shows a large reduction of the delamination kinetics, with the delamination front advancing only 7 mm in 24 h. The shape of the potential profile for the 80-grit sample is similar to the polished and silane-treated samples, but the inhibiting effect on delamination front movement is less profound as is the case for the silane-treated samples. The shape of these potential profiles has been designated as typical for a cathodic delamination mechanism on steel [34,37,44] thereby indicating that cathodic delamination is the responsible delamination mechanism for this system.

The position of the delamination front is determined by the first derivative of the potential and is plotted as a function of the square root of time for three different samples in Fig. 12. From the results it is clear that the polished surface shows very low interfacial stability and low resistance to delamination, indicated by the fast movement of the delamination front over time. Both surface roughening by mechanical
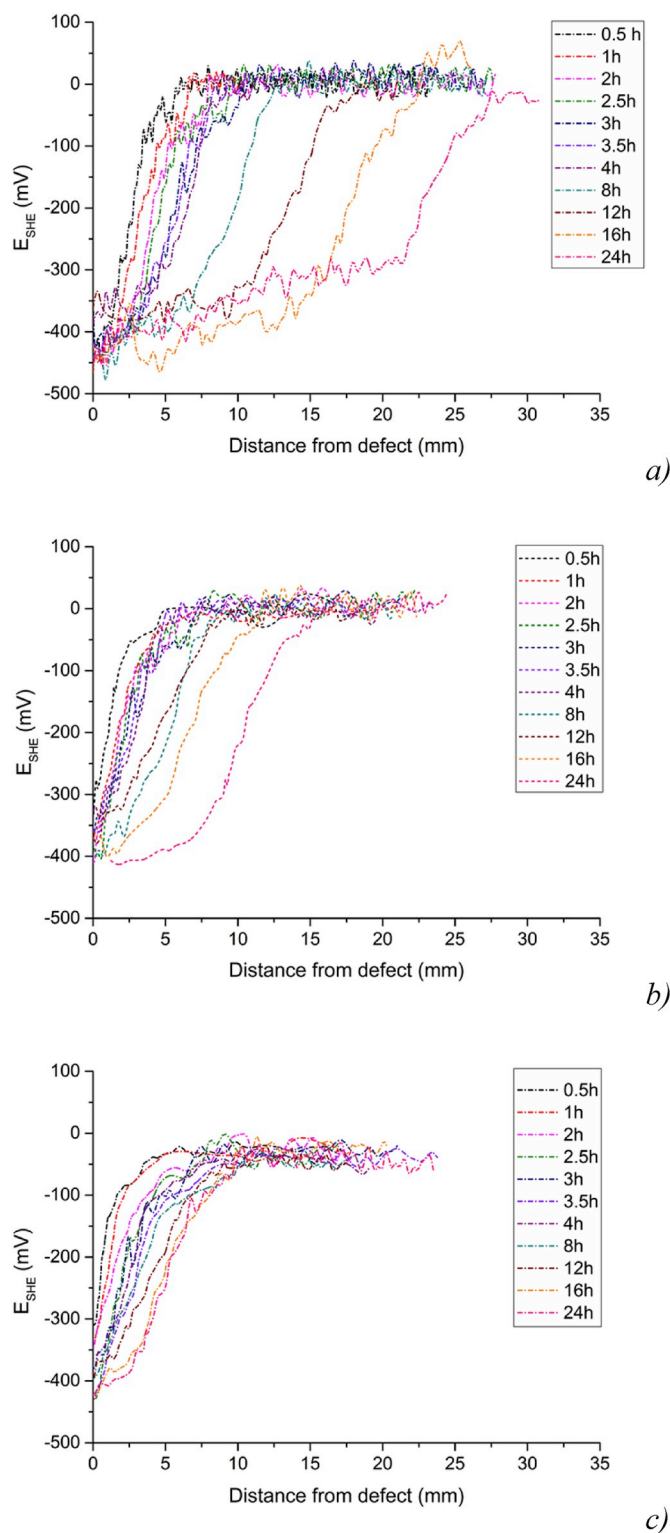

a)

b)

c)

Fig. 11. Potential vs distance from the edge of the defect for different times. (a) polished coated steel, (b) abraded coated steel and (c) silane-treated coated steel. Electrolyte is 3.5 wt% NaCl and humidity was kept at 93% RH.

abrasion and silane pre-treatment significantly decreases the delamination rate of the adhesive film from the steel substrate, thereby showing that both roughness and surface chemistry have a significant contribution to the robustness and hence durability of the adhesion of the steel-epoxy interface. The linear progress of the position of the delamination front with the square root of time indicates that the
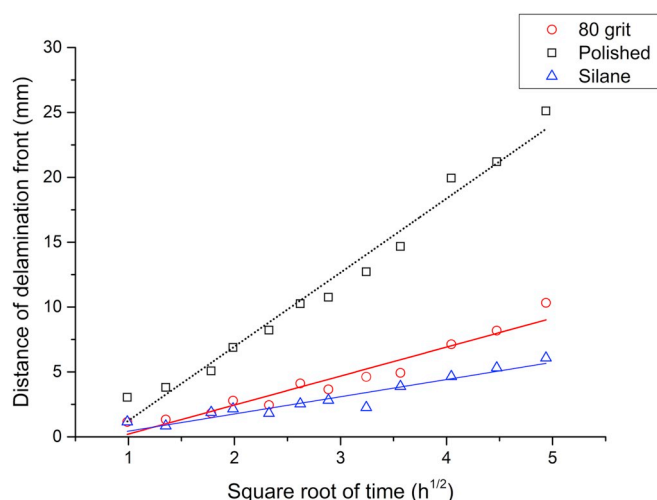
Fig. 12. Delamination front position versus square root of time for polished, 80-grit and silane-treated surfaces.

cathodic delamination process is limited by the cation mobility across the interface [42,43]. The high roughness of the abraded samples creates a long pathway for the electrolyte to diffuse over, thereby limiting the delamination kinetics of the adhesive film. Similar results were found in other studies, highlighting the role of roughness on the delamination kinetics of organic films on steel [12,45]. They concluded that the effect of the surface roughness can be mainly attributed to the increased ionic path along the polymer-steel interface and possibly some minor contribution from possible mechanical interlocking. Our results show that silane treatment is even more effective in decreasing the delamination rate of the adhesive, suggesting that a more stable interface is able to effectively inhibit the mobility of cations. In both cases it can be seen that the enhanced adhesion between the adhesive film and the steel substrate has a significant effect on the kinetics of interfacial delamination. The more profound inhibiting effect of the silane treatment on the delamination kinetics shows resemblance with the performance of the silane-treated specimens in the static wedge test.

4. Conclusions

The aim of this paper was to evaluate the effect of surface chemistry versus surface roughness on the initial adhesion and durability of steel-to-steel adhesively bonded joints. A unique combination of different mechanical tests allowed a detailed evaluation of the joint performance under various environmental and loading conditions. Various pre-treatments were used to alter the surface mechanical or chemical properties. From the single-lap joint shear test it became apparent that roughness of the substrate is the dominant parameter in the initial adhesion between the adhesive and the steel substrates. In addition, specimens with similar average roughness values but altered morphology showed further improvement in the initial adhesion strength. The porous morphologies of the grit blasted and etched surfaces showed superior adhesion performance and appear to be decisive for triggering possible mechanical interlocking. Which results from the formation of a so-called micro-composite interphase zone due to penetration of the adhesive into the surficial pores. Alteration of surface chemistry by zirconium conversion coating or silane treatment, and the associated improved interatomic and intermolecular interactions across the interface compared to untreated polished surfaces, highly improved the initial bond strength for specimens without surface features. These physicochemical contributions were also found to enhance the performance and durability of the adhesive joints after exposure to electrolyte in both loaded and unloaded conditions (static wedge test and scanning Kelvin probe, respectively), thereby reinforcing the importance of a

stable interfacial chemistry to the mechanical performance of the adhesive joint. In both the mechanical tests and the scanning Kelvin probe measurements it was found that surfaces roughened by mechanical abrasion have enhanced bonding areas, leading to an improved initial adhesion but with low resistance to environmental degradation. Conversely, altering the surface chemistry and thereby changing the type of interactions across the interface showed a more significant effect on the interfacial stability during environmental ageing.

References

[1] Brockmann W, Geiß PL, Klingen J, Schröder B. Adhesive bonding - materials. Applications and Technology; 2005. p. 391.

[2] Comyn J. Durability of adhesives in wet conditions. Woodhead Publishing Limited; 2012. https://doi.org/10.1016/B978-1-84569-452-4.50008-4.

[3] Rotella G, Alfano M, Schiefer T, Jansen I. Enhancement of static strength and long term durability of steel/epoxy joints through a fiber laser surface pre-treatment. Int J Adhesion Adhes 2015;63:87–95. https://doi.org/10.1016/j.ijadhadh.2015.08.009.

[4] Mandolfino C, Lertora E, Gambaro C. Effect of surface pretreatment on the performance of adhesive-bonded joints. Key Eng Mater 2013;554–557:996–1006. https://doi.org/10.4028/www.scientific.net/KEM.554-557.996.

[5] Critchlow GW, Webb PW, Tremlett CJ, Brown K. Chemical conversion coatings for structural adhesive bonding of plain carbon steels. Int J Adhesion Adhes 2000;20:113–22. https://doi.org/10.1016/S0143-7496(99)00036-6.

[6] Ghumatkar A, Sekhar R, Budhe S. Experimental study on different adherend surface roughness on the adhesive bond strength. Mater Today Proc 2017;4:7801–9. https://doi.org/10.1016/j.matpr.2017.07.115.

[7] Zielecki W, Pawlus P, PerŁowski R, Dzierwa A. Surface topography effect on strength of lap adhesive joints after mechanical pre-treatment. Arch Civ Mech Eng 2013;13:175–85. https://doi.org/10.1016/j.acme.2013.02.005.

[8] Bennett AR, McMurray HN, Williams G. Optical and SKP studies of corrosion-driven delamination inhibition by polyaniline solid films on iron. ECS Trans 2008;11:71–80. https://doi.org/10.1149/1.2925264. ECS.

[9] Posner R, Giza G, Marazita M, Grundmeier G. Ion transport processes at polymer/oxide/metal interfaces under varying corrosive conditions. Corros Sci 2010;52:1838–46. https://doi.org/10.1016/j.corsci.2010.01.034.

[10] González-Orive A, Giner I, de los Arcos T, Keller A, Grundmeier G. Analysis of polymer/oxide interfaces under ambient conditions – an experimental perspective. Appl Surf Sci 2018;442:581–94. https://doi.org/10.1016/j.apsusc.2018.02.155.

[11] Grothe R, Liu CN, Baumert M, Hesebeck O, Grundmeier G. Scanning Kelvin Probe Blister test measurements of adhesive delamination – bridging the gap between experiment and theory. Int J Adhesion Adhes 2017;73:8–15. https://doi.org/10.1016/j.ijadhadh.2016.11.006.

[12] Khun NW, Frankel GS. Effects of surface roughness, texture and polymer degradation on cathodic delamination of epoxy coated steel samples. Corros Sci 2013;67:152–60. https://doi.org/10.1016/j.corsci.2012.10.014.

[13] Rudawska A. Selected aspects of the effect of mechanical treatment on surface roughness and adhesive joint strength of steel sheets. Int J Adhesion Adhes 2014;50:235–43. https://doi.org/10.1016/j.ijadhadh.2014.01.032.

[14] Wielant J, Posner R, Hausbrand R, Grundmeier G, Terryn H. SKP as a tool to study the physicochemical interaction at buried metal-coating interfaces. Surf Interface Anal 2010;42:1005–9. https://doi.org/10.1002/sia.3512.

[15] Sababi M, Terryn H, Mol JMC. The influence of a Zr-based conversion treatment on interfacial bonding strength and stability of epoxy coated carbon steel. Prog Org Coat 2017;105:29–36. https://doi.org/10.1016/j.porgcoat.2016.11.016.

[16] Tchoquessi Doidjo MR, Belec L, Aragon E, Joliff Y, Lanarde L, Meyer M, et al. Influence of silane-based treatment on adherence and wet durability of fusion bonded epoxy/steel joints. Prog Org Coat 2013;76:1765–72. https://doi.org/10.1016/j.porgcoat.2013.05.014.

[17] Li G, Wang X, Li A, Wang W, Zheng L. Fabrication and adhesive properties of thin organosilane films coated on low carbon steel substrates. Surf Coat Technol 2007;201:9571–8. https://doi.org/10.1016/j.surfcoat.2007.04.032.

[18] Wielant J, Hauffman T, Blajiev O, Hausbrand R, Terryn H. Influence of the iron oxide acid-base properties on the chemisorption of model epoxy compounds studied by XPS. J Phys Chem C 2007;111:13177–84. https://doi.org/10.1021/jp072354j.

[19] Kozma L, Olefjord I. Surface treatment of steel for structural adhesive bonding. Mater Sci Technol 1987;3:954–62. https://doi.org/10.1179/mst.1987.3.11.954.

[20] Johnsen BB, Olafsen K, Stori A. Reflection-absorption FT-IR studies of the specific interaction of amines and an epoxy adhesive with GPS treated aluminium surfaces. Int J Adhesion Adhes 2003;23:155–63. https://doi.org/10.1016/S0143-7496(03)00008-3.

[21] Yang L, Feng J, Zhang W, Qu J-E. Film forming kinetics and reaction mechanism of Î³-glycidoxypropyltrimethoxysilane on low carbon steel surfaces. Appl Surf Sci 2010;256:6787–94. https://doi.org/10.1016/j.apsusc.2010.04.090.

[22] Valenza A, Fiore V, Fratini L. Mechanical behaviour and failure modes of metal to composite adhesive joints for nautical applications. Int J Adv Manuf Technol 2011;53:593–600. https://doi.org/10.1007/s00170-010-2866-1.

[23] Asemani HR, Ahmadi P, Sarabi AA, Eivaz Mohammadloo H. Effect of zirconium conversion coating: adhesion and anti-corrosion properties of epoxy organic coating containing zinc aluminum polyphosphate (ZAPP) pigment on carbon mild steel. Prog Org Coat 2016;94:18–27. https://doi.org/10.1016/j.porgcoat.2016.01.015.

[24] International Organization for Standardization. ISO 25178- 2:2012 geometrical product specifications (GPS)—surface texture: areal—Part 2: terms definitions and surface texture parameters. 2012.

[25] da Silva LFM, Carbas RJC, Critchlow GW, Figueiredo MAV, Brown K. Effect of material, geometry, surface treatment and environment on the shear strength of single lap joints. Int J Adhesion Adhes 2009;29:621–32. https://doi.org/10.1016/j.ijadhadh.2009.02.012.

[26] Goglio L, Rezaei M. Degradation of epoxy-steel single lap joints immersed in water. J Adhes 2015;91:621–36. https://doi.org/10.1080/00218464.2014.948614.

[27] Khan MH, Gali OA, Edrisy A, Riahi AR. Effect of oxidation and surface roughness on the shear strength of single-lap-joint adhesively bonded metal specimens by tension loading. Appl Adhes Sci 2016;4:21. https://doi.org/10.1186/s40563-016-0077-1.

[28] Adams RD, Cowap JW, Farquharson G, Margary GM, Vaughn D. The relative merits of the Boeing wedge test and the double cantilever beam test for assessing the durability of adhesively bonded joints, with particular reference to the use of fracture mechanics. Int J Adhesion Adhes 2009;29:609–20. https://doi.org/10.1016/j.ijadhadh.2009.02.010.

[29] Banea MD, da Silva LFM, Campilho RDSG. Moulds design for adhesive bulk and joint specimens manufacturing. Assemb Autom 2012;32:284–92. https://doi.org/10.1108/01445151211244456.

[30] Warren DJ, McMurray HN, de Vooys ACA. Localised SKP studies of cathodic disbondment on chromium/chromium oxide coated steel. ECS Trans 2013;50:67–78. https://doi.org/10.1149/05047.0067ecst.

[31] Leng A, Streckel H, Stratmann M. The delamination of polymeric coatings from steel. Part 1: calibration of the Kelvinprobe and basic delamination mechanism. Corros Sci 1998;41:547–78. https://doi.org/10.1016/S0010-938X(98)00166-8.

[32] Poorna Chander K, Vashista M, Sabiruddin K, Paul S, Bandyopadhyay PPP. Effects of grit blasting on surface properties of steel substrates. Mater Des 2009;30:2895–902. https://doi.org/10.1016/j.matdes.2009.01.014.

[33] Patel K, Doyle CS, Yonekura D, James BJ. Effect of surface roughness parameters on thermally sprayed PEEK coatings. Surf Coat Technol 2010;204:3567–72. https://doi.org/10.1016/j.surfcoat.2010.04.026.

[34] Pohl K, Ozcan O, Voigt M, Grundmeier G. Adhesion and corrosive delamination of epoxy films on chemically etched ZnMgAl-alloy coatings. Mater Corros 2016;67:1020–6. https://doi.org/10.1002/maco.201608968.

[35] Jang JJ, Kim EK. Corrosion protection of epoxy-coated steel using different silane coupling agents. J Appl Polym Sci 1999;71:585–93. https://doi.org/10.1002/(SICI)1097-4628(19990124)71:4<585. AID-APP10>3.0.CO;2-D.

[36] Fockaert LI, Taheri P, Abrahami ST, Boelen B, Terryn H, Mol JMC. Zirconium-based conversion film formation on zinc, aluminium and magnesium oxides and their interactions with functionalized molecules. Appl Surf Sci 2017;423:817–28. https://doi.org/10.1016/j.apsusc.2017.06.174.

[37] Reichinger M, Bremser W, Dornbusch M. Interface and volume transport on technical cataphoretic painting: a comparison of steel, hot-dip galvanised steel and aluminium alloy. Electrochim Acta 2017;231:135–52. https://doi.org/10.1016/j.electacta.2017.02.013.

[38] Özdemir A, Kocabaş İ, Svanda P. Improving the strength of adhesively bonded joints through the introduction of various surface treatments. J Adhes Sci Technol 2016;30:2573–95. https://doi.org/10.1080/01694243.2016.1188872.

[39] Brack N, Rider ANN. The influence of mechanical and chemical treatments on the environmental resistance of epoxy adhesive bonds to titanium. Int J Adhesion Adhes 2014;48:20–7. https://doi.org/10.1016/j.ijadhadh.2013.09.012.

[40] Harris AF, Beevers A. Effects of grit-blasting on surface properties for adhesion. Int J Adhesion Adhes 1999;19:445–52. https://doi.org/10.1016/S0143-7496(98)00061-X.

[41] Stratmann M, Leng A, Fürbeth W, Streckel H, Gehmecker H, Große-Brinkhaus K-H. The scanning Kelvin probe; a new technique for the in situ analysis of the delamination of organic coatings. Prog Org Coat 1996;27:261–7. https://doi.org/10.1016/0300-9440(94)00542-7.

[42] Rohwerder M, Frankel GS, Stratmann M, Leblanc P. Application of scanning kelvin probe in corrosion science. Anal Methods Corros Sci Eng 2010:605–48. https://doi.org/10.1201/9781420028331.ch16.

[43] Leng A, Streckel H, Stratmann M. The delamination of polymeric coatings from steel. Part 2: first stage of delamination, effect of type and concentration of cations on delamination, chemical analysis of the interface. Corros Sci 1998;41:579–97. https://doi.org/10.1016/S0010-938X(98)00167-X.

[44] Wielant J, Posner R, Hausbrand R, Grundmeier G, Terryn H. Cathodic delamination of polyurethane films on oxide covered steel - combined adhesion and interface electrochemical studies. Corros Sci 2009;51:1664–70. https://doi.org/10.1016/j.corsci.2009.04.014.

[45] Sørensen PA, Dam-Johansen K, Weinell CE, Kiil S. Cathodic delamination: quantification of ionic transport rates along coating-steel interfaces. Prog Org Coat 2010;67:107–15. https://doi.org/10.1016/j.porgcoat.2009.10.011.